BJR

https://doi.org/10.1259/bjr.20190400

Received: 30 April 2019 | Revised: 29 February 2020 | Accepted: 09 March 2020

Cite this article as:
Jiang J, Fu Y, Hu X, Cui L, Hong Q, Gu X, et al. The value of diffusion-weighted imaging based on monoexponential and biexponential models for the diagnosis of benign and malignant lung nodules and masses. *Br J Radiol* 2020; **93**: 20190400.

FULL PAPER

The value of diffusion-weighted imaging based on monoexponential and biexponential models for the diagnosis of benign and malignant lung nodules and masses

[1]JIANQIN JIANG, [1]YIGANG FU, [2]XIAOYUN HU, [3]LEI CUI, [1]QIN HONG, [4]XIAOWEN GU, [3]JIANBING YIN, [3]RONGFANG CAI and [1]GAOFENG XU

[1]Department of Radiology, Yancheng City No.1 People's Hospital, Yancheng, China
[2]Department of Radiology, Wuxi People's Hospital, Wuxi, China
[3]Department of Radiology, Second Affiliated Hospital of Nantong University, Nantong, China
[4]Department of Radiology, Suzhou Municipal Hospital, Suzhou, China

Address correspondence to:
Lei Cui
E-mail: *cuigeleili@126.com*
Gaofeng Xu
E-mail: *18905100082@163.com*

The authors Jianqin Jiang and Yigang Fu contributed equally to the work.

Objectives: The objective is to compare the efficacy of diffusion-weighted imaging (DWI) parameters of mean and minimum apparent diffusion coefficient (ADC_{mean} and ADC_{min}) and intravoxel incoherent motion (IVIM) in the differentiation of benign and malignant lung nodules and masses.

Methods: Lung lesions measured larger than 1.5 cm on CT were included between August 2015 and September 2018. DWI (10 b-values, 0–1000 s/mm^2) scans were performed, and the data were post-processed to derive the ADC_{mean}, ADC_{min} and IVIM parameters of true diffusion coefficient (D), pseudodiffusion coefficient (D*) and perfusion fraction (f). An independent sample *t*-test or Mann–Whitney *U* test was used to compare benign and malignant parameters. Receiver operating characteristic curves were generated and a *Z* test was used.

Results: 121 patients were finally enrolled, each with one lesion. Examined 121 lesions were malignant in 88 (72.7%) and benign in 33 (27.3%). The ADC_{mean} of malignant pulmonary nodules was significantly lower than that of benign pulmonary nodules (t = 3.156, p = 0.006), whereas the other parameters revealed no significant differences (p = 0.162–0.690). Receiver operating characteristic curve analysis revealed that an ADC_{mean} threshold value of 1.43 × 10^{-3} mm^2/s yielded 88.57% sensitivity and 64.29% specificity. While for lung masses, the ADC_{mean}, ADC_{min}, D and D* values in malignant pulmonary masses were significantly lower (P<0.001–0.011). Among them, the D value exhibited the best diagnostic performance when the threshold of D was 1.23 × 10^{-3}mm^2/s, which yielded a sensitivity of 90.57% and a specificity of 89.47% (Z = 2.230, 3.958, 2.877 and p = 0.026, <0.001 and 0.004, respectively).

Conclusion: ADC is the most robust parameter to differentiate benign and malignant lung nodules, whereas D is the most robust parameter to differentiate benign and malignant lung masses.

Advances in knowledge: This is the first study to compare all the quantitative parameters of DWI and IVIM mentioned in the literatures for assessing lung lesions; Second, we divided the lesions into lung nodules and lung masses with the size of 3 cm as the boundary.

INTRODUCTION

The diagnosis of pulmonary nodules and masses remains a challenge in clinical practice. CT is currently the preferred imaging technique; however, diagnosis by CT is still based on morphological criteria. Contrast-enhanced CT can obtain information regarding blood perfusion; however, this method has limited specificity in the presence of active granulomas and hypervascular lesions.[1] Other imaging methods include CT perfusion (CTP), positron emission tomography-CT (PET-CT), and dynamic contrast-enhanced MRI (DCE-MRI). Though these techniques have

their own advantages, they all require an injection of contrast medium.

Diffusion-weighted MRI (DW-MRI) is a radiation-free and contrast-free functional imaging technique that quantitatively evaluates the motion of water molecules within tissue. It has been reported that the quantitative parameter of the apparent diffusion coefficient (ADC) has the potential to differentiate benign and malignant lung lesions[2–5]; however, ADC is influenced by both diffusion and perfusion effects. Conversely, the biexponential model of DWI, the intravoxel incoherent motion (IVIM), can distinguish between molecular diffusion and microcirculation perfusion to obtain the true diffusion coefficient (D), pseudo diffusion coefficient (D*), and perfusion fraction (f).[6]

Recently, interest has grown in discussing the application of DWI- and IVIM-derived parameters in the identification of benign and malignant lung lesions. Often, different studies have used different parameters, resulting in varied outcomes.[1,7,8] Weller[9] et al and Jiang[10] et al suggested that the size of the lesions was the influencing factor that led to the measurement variability of ADC and IVIM parameter values in lung cancer. Thus, we hypothesised that the lesion size may also affect the diagnostic performance of ADC and IVIM parameters. Furthermore, it remains to be clarified whether the diagnostic index and cut-off values for smaller size lung nodules and larger size lung masses are the same.

Therefore, we aimed to evaluate the efficiency of the mean and minimum ADC values (ADC_{mean} and ADC_{min}) and the IVIM parameters D, D*, and f in the diagnosis of pulmonary nodules and masses, with the goal of providing a theoretical basis for the clinical evaluation of pulmonary nodules and masses by these parameters.

METHODS AND MATERIAL

Patients

The local Research Ethics Committee approved this study, and informed consent was obtained from each patient. Inclusion criteria were as follows: (1) the maximum tumour diameter measured >1.5 cm on conventional thin-section area-detector CT scans (Siemens 64-slice SOMATOM Definition Flash dual-source CT) obtained with a lung window setting, and the ground glass, calcification, necrosis, and cavity components of the tumour measured less than one-third of the lesion; (2) the patient received no prior antitumour treatment or invasive examinations such as puncture biopsy or bronchoscopy, and histopathological findings were obtained within 1 month of MR examination; and (3) absence of MRI examination contraindications. From August 2015 to September 2018, eligible patients were included in the study for MR examination.

MR imaging protocols

All MRI examinations were performed on a 3 T MR scanner (Verio Tim; Siemens, Erlangen, Germany) with 8-channel phased array surface coils and with the patients in the head-first supine position. The abdominal belt was used to compensate respiratory motion artefacts. Scan sequences included routine MR plain scan and DWI scans: (1) coronal single-shot fast-spin echo breath-hold T_2 weighted imaging (WI): repetition time (TR) 1200 ms, echo time (TE) 83 ms, matrix 288 × 288, field of view (FOV) 36 × 36 cm, slice thickness 6 mm, interslice gap 7.2 mm, and 20-slice scanning; (2) axial fat-suppressed respiratory-triggered T_2WI: TR 2000 ms, TE 90 ms, matrix 320 × 320, FOV 36 × 36 cm, slice thickness 5 mm, inter slice gap 6.5 mm, and 28-slice scanning; (3) axial fat-suppressed breath-hold T_1WI: TR 4.22 ms, TE 1.9 ms, matrix 384 × 384, FOV 38 × 38 cm, slice thickness 3 mm, interslice gap 0.6 mm, and 64-slice scanning; and (4) axial free-breathing single-shot spin echo DWI: b values of 0, 50, 100, 150, 200, 250, 300, 500, 800, 1000 s/mm^2, TR 7600 ms, TE 67 ms, matrix 128 × 160, FOV 36 × 31 cm, slice thickness 6 mm, interslice gap 0.6 mm, receiver bandwidth 2442 Hz/pixel, parallel factor 2 (performed by using k-space algorithm (generalised autocalibrating partially parallel acquisition, GRAPPA, Siemens).[11]

Image analysis

DWI data were post-processed with mono- and biexponential models.

ADC

For the monoexponential model, ADC maps were generated on the Siemens post-processing workstation (syngoMMWP) using all 10 b-values based on the equation $S_b = S_0 exp\ (-bADC)$. S_0 and S_b represent the signal intensities at a b value of 0 s/mm^2 and a specified b value, respectively. Then, the ADC_{mean} and ADC_{min} values were obtained meanwhile from drawing one region of interest (ROI) at the level of maximum transverse diameter of the tumour on ADC maps. ROI was manually outlined along the edge of the lesion including the solid components as much as possible and visually identified calcifications, large vessels, necrosis areas, and artifacts were excluded by referring to CT and MR images.[8,12,13] Three times of measurements were performed, and the ADC_{mean} and ADC_{min} were the average values of three measurements.

IVIM

For the biexponential model, IVIM data were processed offline with an in-house software, the open-source medical imaging interaction toolkit MITK[10,14,15](MITK Diffusion, v. 2014; DKFZ, Heidelberg, Germany) (http://mitk.org/wiki/MITK). The process was based on the following equations[16]:

$$S_b/S_0 = e\,bD \quad (1)$$

$$S_b/S_0 = fe^{-bD^*} + (1\,f)e^{-bD} \quad (2)$$

where f is the fraction of perfusion, D is the diffusion coefficient representing pure molecular diffusion, and D* is the pseudo-diffusion coefficient representing blood microcirculation perfusion in the capillary network. The contribution of D* to signal attenuation can be neglected at higher b values (typically above 200 s/mm^2).[12,16,17] Thus, the curve was fitted for high b values to the single parameter of D[17] (using Eq. 1). Subsequently, with D as a constant, the curve was fitted for f and D* to all b values[17] (using Eq. 2). Then, the f and D* values were automatically calculated. The ROIs were kept as close as possible to those on ADC

maps. The parameters were also measured thrice, and the average values were recorded.

Two radiologists (observers A and B, with 5 and 10 years of experience in MRI reading, respectively) independently measured and recorded the parameters. After an interval of 2 weeks, each radiologist performed the second analysis.

Statistical analysis

Statistical analysis was performed using SPSS 20.0 (IBM, Chicago, IL) and MedCalc 12.3.0 (Mariakerke, Belgium). Interobserver reproducibility was assessed with an interclass correlation coefficient (ICC), and the agreement was considered good when the ICC >0.75. All parameters were tested for normal distribution using the Kolmogorov–Smirnov test. Independent sample *t*-tests (normal distribution) or Mann–Whitney *U* tests (non-normal distribution) were used to compare the differences between the parameters in benign and malignant lung nodules and masses. Receiver operating characteristic (ROC) curves were generated to evaluate the parameters' performances in the diagnosis of lung lesions and to identify the cut-off values. We determined the optimal threshold values resulting in the highest accuracy. A *Z* test was used to compare the differences in the areas under the ROC curves (AUCs). A *p*-value less than 0.05 was considered significant.

RESULTS

From August 2015 to September 2018, 131 consecutive patients were initially recruited. Among them, patients with pathology confirmed lung abscesses ($n = 3$) and images with poor quality which demonstrated serious geometric distortion and artefacts ($n = 7$)[10]were excluded. The remaining 121 patients including 74 males and 47 females (mean age 60.2 years; range, 21–80 years) were finally enrolled, each with one lesion. The average lesion size was 3.72 ± 1.71 cm (range, 1.5–9.0 cm). There are 49 lung nodes and 72 lung masses with a size of 3 cm as the boundary.[18] All lesions were confirmed by pathological examination: 54 cases by surgery, 31 cases by percutaneous lung biopsy, 34 cases by fibreoptic bronchoscopy biopsy, and two cases by identification of cancer cells in pleural effusion. The patients confirmed as benign cases were followed up for at least 6 months. A total of 88 malignant tumours and 33 benign tumours were observed. Table 1 summarises the detailed pathological characteristics of these lesions.

Intra- and Interobserver reproducibility

All parameters revealed good intra- and interobserver agreement, except for D* (ICC 0.745). The intraobserver ICCs of the ADC_{mean}, ADC_{min}, D, D*, and f values are 0.970, 0.810, 0.931, 0.869 and 0.844, respectively. The interobserver ICCs of the ADC_{mean}, ADC_{min}, D, D*, and f values are 0.862, 0.758, 0.919, 0.745 and 0.803, respectively.

Differences in parameters between benign and malignant pulmonary nodules

The ADC_{mean} of malignant pulmonary nodules was significantly lower than that of benign pulmonary nodules ($t = 3.156$, $p = 0.006$). In contrast, the ADC_{min}, D, D* and f values revealed no significant differences between benign and malignant pulmonary nodules ($p = 0.162$–0.690) (Table 2).

Differences in parameters between benign and malignant pulmonary masses

The ADC_{mean}, ADC_{min}, D and D* values of malignant pulmonary masses were significantly lower than those of benign pulmonary

Table 1. The detailed pathological results of lesions

		Lung nodes ($n = 49$)	Lung masses ($n = 72$)
Malignant ($n = 88$)	Adenocarcinoma	22	29
	Squamous cell carcinoma	5	14
	Small-cell lung cancer	3	6
	Undifferentiated type of non-small cell lung cancer	4	1
	Lymphoid epithelioid carcinoma	1	
	Pulmonary MALT lymphoma		1
	Large cell neuroendocrine tumor		1
	Metastasis		1
Benign ($n = 33$)	Tuberculoma	2	3
	Organised pneumonia	4	7
	Granuloma	3	
	Fungal infections		6
	Sclerosing pneumocytoma	4	2
	Inflammatory pseudotumor	1	
	Bronchial cyst		1

MALT, mucosa-associated lymphoid tissue.

Table 2. Difference of parameters between benign and malignant pulmonary nodules and masses

		ADC_{mean} ($\times10^{-3}$ mm^2/s)	ADC_{min} ($\times10^{-3}$ mm^2/s)	D ($\times10^{-3}$ mm^2/s)	D* ($\times10^{-3}$ mm^2/s)	f (%)
Lung nodules (n = 49)	Malignant (n = 35)	1.18 ± 0.22[b]	0.62 ± 0.19[b]	1.11 ± 0.25[b]	16.89 ± 16.14[c]	18.95 ± 10.92[b]
	Benign (n = 14)	1.52 ± 0.38[b]	0.67 ± 0.28[b]	1.30 ± 0.44[b]	12.67 ± 8.44[c]	23.25 ± 9.36[b]
	t/Z	3.156	0.597	1.463	−0.399	1.293
	P	0.006	0.558	0.162	0.690[a]	0.202
Lung masses (n = 72)	Malignant (n = 53)	1.19 ± 0.22[b]	0.63 ± 0.24[b]	1.00 ± 0.22[b]	11.43 ± 7.45[c]	17.71 ± 10.13[b]
	Benign (n = 20)	1.78 ± 0.64[b]	0.83 ± 0.37[b]	1.55 ± 0.51[b]	22.21 ± 13.96[b]	22.23 ± 13.88[b]
	t/Z	−3.954	2.662	4.536	−2.529	1.843
	P	0.001	0.010	<0.001	0.011[a]	0.070

ADC, apparent diffusion coefficient.
[a]Mann–Whitney U test, the rest are independent sample t-tests. $p < 0.05$ considered statistically significant.
[b]Parameter values showed a normal distribution, expressed as means ± standard deviations.
[c]Parameter values showed a nonnormal distribution, expressed as medians ± interquartile ranges.

masses (P<0.001–0.011); however, no significant difference was observed in the f values of benign and malignant lung masses (p = 0.070) (Table 2).

The efficacy of ADC_{mean} in the diagnosis of benign and malignant pulmonary nodules

ROC curve analysis revealed that when the cut-off value of ADC_{mean} was 1.43×10^{-3} mm^2/s, the area under the curve (AUC) in diagnosing benign and malignant pulmonary nodules was 0.769, with a sensitivity and specificity of 88.57% and 64.29%, respectively. According to this threshold, ADC can correctly diagnose 85.71% (30/35) of malignant pulmonary nodules and 64.29% (9/14) of benign pulmonary nodules. A representative case of lung nodules is shown in Figure 1 and a representative false-positive case is shown in Figure 2.

The efficacy of the ADC_{mean}, ADC_{min}, D, and D*Values in the diagnosis of benign and malignant pulmonary masses

The results of ROC curves for ADC_{mean}, ADC_{min}, D and D* values in lung masses are illustrated in Figure 3 and Table 3. ROC curve analysis showed that the D value had the largest AUC (0.882) when the threshold of D was 1.23×10^{-3}mm^2/s, resulting in a sensitivity of 90.57% and a specificity of 89.47%. Conversely, the ADC_{mean}, ADC_{min} and D* values demonstrated inferior diagnostic performances compared to the D value, with AUCs of 0.805, 0.667 and 0.696, respectively (Z = 2.230, 3.958, 2.877 and p = 0.026, <0.001 and 0.004, respectively). According to the threshold of D and ADC, D can correctly diagnose 88.68% (47/53) of malignant pulmonary masses and 89.47% (17/19) of benign pulmonary masses, and ADC can correctly diagnose 92.45% (49/53) of malignant pulmonary masses and 63.16% (12/19) of benign pulmonary masses. A representative case of lung masses is shown in Figure 4.

DISCUSSION

In malignant tumours, increased cellular proliferation and decreased extracellular space restrict the diffusion of water molecules, and DWI is characterised by high signal intensity while the ADC map shows relatively low signal intensity.[8,19]Therefore, as reported previously, the ADC value of a malignant tumour is lower than that of a benign tumour.[5,8,13,20] Meta-analyses have also confirmed the result in lung cancer.[2–4] In the present study, we performed separate comparisons in lung nodules and masses and found that the ADC mean value demonstrated good diagnostic performance in both lesion types, a result which is in accordance with those of previous studies.[5,7,8,13,21] Further, the present research[9,10,22] on repeatability has shown the ADC value to be well-replicated, indicating that the ADC_{mean} is a relatively stable and clinically viable diagnostic parameter.

At present, there were also studies[23,24] based on the assumption that the ADC_{min} would more accurately represent the most invasive components within tumours. Çakmak[23] et al and Usuda[24] et al found a higher diagnostic capability of ADC_{min} in assessing pulmonary lesions compared to lesion-to spinal cord signal intensity ratio (LSR) and PET. However, in this study, ADC_{min} was found to be a relatively poor diagnostic index. These results presumably reflect the fact that ADC_{min} is an extreme value and is thus easily influenced by variations in measurement and susceptible to partial volume effects. Volumetric-based histogram analysis may reduce measurement variability,[25,26] and Yuan[26] et al demonstrated that histogram analysis of ADC_{10th} showed significantly higher AUC values than mean ADC, indicating that histogram metrics could be a more promising method for assessing lung nodules and masses.

Theoretically, D is more accurate than ADC in probing water molecule diffusion in tumours. Studies by Yuan[20,26] et al and Wan[8] et al have confirmed the greater diagnostic value of D in lung cancer; however, Koyama et al[1] and Deng et al[7] have reported

Figure 1. A representative case of pulmonary nodules. A 57-year-old male confirmed as granulomattis in the right lower lung zone by surgery. (a) CT image. (b) DWI image (b = 800 s/mm^2). (c) ADC map. (d) IVIM-D map. (e) IVIM-D* map. (f) IVIM-f map. (g) The generated curve of IVIM. (h) Photomicrograph of the lesion (HE × 200). The measured $ADC_{mean}$was 1.54 × 10^{-3} mm^2/s, which was greater than the cut-off value 1.40 × 10^{-3} mm^2/s and thus indicated a benign tumour. Conversely, the measured D value was 0.98 × 10^{-3} mm^2/s, which cannot conclusively diagnose a benign nodule. In this case, the data fitting of the IVIM curve (d), particularly for D* and f, may be inaccurate due to the presence of outliers. ADC, apparent diffusion coefficient; DWI, diffusion-weighted imaging; IVIM, intravoxel incoherent motion.

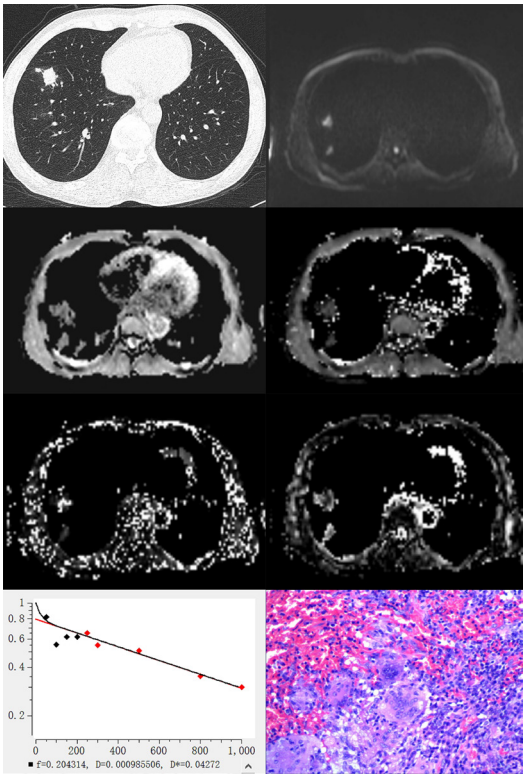

Figure 2. A representative false-positive case. A 61-year-old male confirmed as organic pneumonia in the right lower lung zone by surgery. (a) CT image. (b) DWI image (b = 800 s/mm^2). (c) ADC map. (d) IVIM-D map. (e) IVIM-D* map. (f) IVIM-f map. (g) The generated curve of IVIM. (h) Photomicrograph of the lesion (HE × 200). The measured ADC and D values were 1.06 × 10^{-3} mm^2/s and 0.93 × 10^{-3} mm^2/s, respectively, which were both lower than the cut-off values. The photomicrograph indicated that the alveoli were compressed, and a large number of lymphocytes had infiltrated the lesion. ADC,apparent diffusion coefficient; DWI, diffusion-weighted imaging; IVIM, intravoxel incoherent motion.

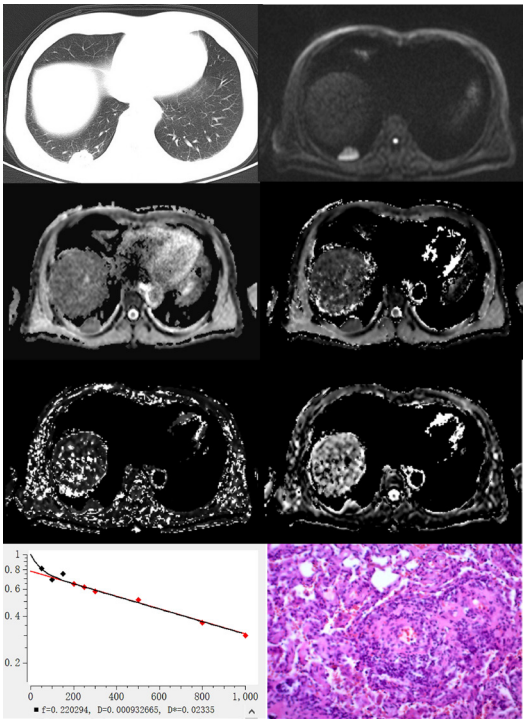

Figure 3. ROC curves for ADC_{mean}, ADC_{min}, D and D* values in the diagnosis of benign and malignant pulmonary masses. The AUCs of ADC_{mean}, ADC_{min}, D and D* were 0.805, 0.667, 0.882 and 0.696, respectively. The D value under the largest AUC when the threshold of D was set to 1.23 × 10^{-3}mm^2/s, with a sensitivity of 90.57% and a specificity of 89.47% (Z = 2.230, 3.958, 2.877 and p = 0.026, <0.001 and 0.004, respectively). ADC, apparent diffusion coefficient; AUC, area under the curve; ROC, receiver operating characteristic.

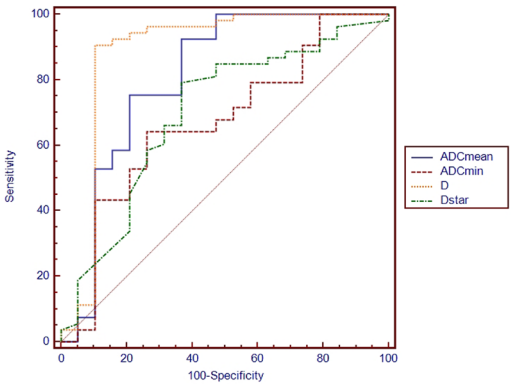

that D was insufficient in the differential diagnosis, and Wan[27] et al found that D has similar diagnostic ability compared with conventional ADC. In the present study, the D value performed better than the ADC mean value in larger size lung masses. Nevertheless, no significant differences were observed in the D values of benign and malignant lung nodules, suggesting that the size of the lesion may influence the diagnostic performance. This result could be interpreted as evidence that, similar to the ADC value, the D value is also vulnerable to motion and susceptibility artifacts and the partial volume effect.[1,10] We hypothesised that these effects were particularly evident in smaller size lung lesions. Electrocardiogram (ECG) gating can potentially avoid pulsation artefacts, but this technique is time-consuming and is not commonly used in clinical practice.[28,29] Weller et al[9] proposed that respiratory motion has a greater impact on smaller lesions, and in the future the use of motion compensation protocols may be warranted when assessing small lesions. Further, Koyama[1] et al reported that obtaining multiple b values for IVIM

Table 3. Results of ROC curve analysis of malignant pulmonary masses

	Thresholds	AUC	Sensitivity	Specificity
ADC_{mean}	$1.46 \times 10^{-3} mm^2/s$	0.805 (0.665–0.866)	92.45%	63.16%
ADC_{min}	$0.67 \times 10^{-3} mm^2/s$	0.667 (0.528–0.757)	64.15%	73.68%
D	$1.23 \times 10^{-3} mm^2/s$	0.882 (0.755–0.928)	90.57%	89.47%
D*	$15.9 \times 10^{-3} mm^2/s$	0.696 (0.555–0.780)	79.25%	63.16%

ADC, apparent diffusion coefficient; AUC, area under the curve; ROC, receiver operating characteristic.

curves is time-consuming and error-prone. Taking these factors into consideration, the utility of IVIM parameters in the diagnosis of small size lung nodules in clinical practice is still worth discussing.

Figure 4. A representative case of pulmonary masses. A 58-year-old male confirmed as squamous cell carcinoma in the left lower lung zone by surgery. (a) CT image. (b) DWI image (b = 800 s/mm^2). (c) ADC map. (d) IVIM-D map. (e) IVIM-D* map. (f) IVIM-f map. (g) The generated curve of IVIM. (h) Photomicrograph of the lesion (HE × 200). The measured D value was 1.21 × 10^{-3} mm^2/s, indicating a malignant tumour, whereas the measured ADC_{mean} (1.56 × 10^{-3} mm^2/s) was obviously higher, suggesting that it was influenced by the perfusion effect. ADC, apparent diffusion coefficient; DWI, diffusion-weighted imaging; IVIM, intravoxel incoherent motion.

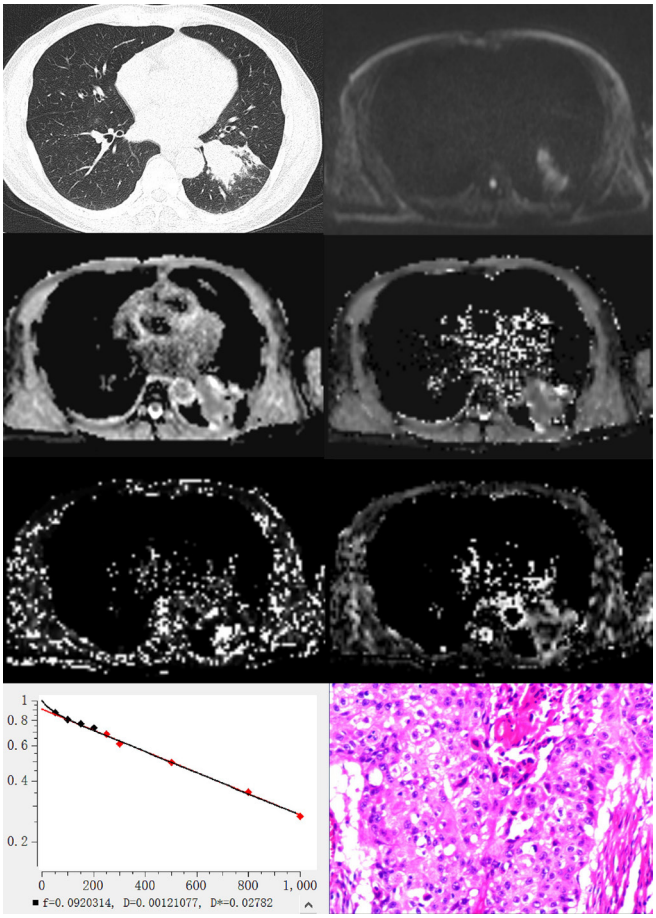

This study showed that the threshold of ADC for the diagnosis of benign and malignant lung nodules and masses was 1.43 × 10^{-3} and 1.46 × 10^{-3} mm^2/s, respectively, and the threshold of D was 1.23 × 10^{-3} mm^2/s. These results fall within the range reported in the literature, although the cut-off values used in different studies vary.[1,2,8,21] This variability may be related to inconsistencies in the sample size, scanning equipment, sequences and post-processing methods of different studies. 3 T MRI was used in this study. The magnetic field inhomogeneity and magnetic susceptibility artefacts in 3 T MRI are higher than those in 1.5 T MRI. However, the combination of parallel acquisition technology can accelerate image acquisition and reduce DWI artefacts. At the same time, the choice of b values affects the generation of ADC and D maps. However, there is no uniform standard for the selection of b values in current studies. Future research needs to acquire consistency in these aspects to ensure similar results across multiple institutions.

In the present research, according to the thresholds, ADC and D diagnosed most malignant nodules (ADC, 30/35) and masses (ADC, 49/53 and D, 47/53). However, for benign lesions, the diagnostic efficiency of ADC (lung nodules, 9/14 and lung masses, 12/19) and D (lung masses, 17/19) decreased, with the ADC values exhibiting a particularly striking decrease. The ADC value has been shown to be ineffective in the diagnosis of tuberculosis, organic pneumonia, fungal infection and granuloma. The lower diagnostic efficacy of ADC in these diseases may result from extravasation and inflammatory cell infiltration, purulent exudate, fibrous tissue hyperplasia, and increased cell viscosity, which impede the diffusion of water molecules and cause their ADC or D values to decrease and overlap with those of malignant lesions.[7,8]

The IVIM perfusion fraction (f) is the volume of the capillary network detected by MRI, and thus, f mainly represents the blood volume.[6] Deng[7] et al and Wang[12] et al found that the f value of localised inflammatory lesions and obstructive pulmonary consolidation was significantly higher than that of malignant lung tumours. Other studies suggested that f was ineffective in differentiating between benign and malignant lung lesions.[1,8,20,26] In our study, benign and malignant cases did not exhibit significant differences in their f values. The inconsistencies between these studies may be associated with the diverse pathological types enrolled in each study. For example, in the Deng[7] et al study, three of the eight benign cases were diagnosed by the disappearance or significant regression of the nodules after anti-inflammatory treatment, and the Wang[12] et al study included

obstructive lung consolidation. These lesions are usually characterised by exudative inflammation, including vasodilation, increased permeability, and increased blood flow. Therefore, the authors observed higher f values reflecting the elevated blood perfusion in these subjects. However, other studies, such as the study performed by Wan[8] et al and the present work, predominantly included chronic inflammation or benign lung tumours in which the vascular changes were not apparent as neovascularization in malignant tumours. Additionally, f is influenced by TE, T2 contribution and relaxation effects,[7,30] and other bulk flow phenomena can also cause signal attenuation at lower b values and may be difficult to distinguish from perfusion effects.[16] Studies[10,31] have also reported poor measurement reproducibility of D* and f, especially D*, which can be reflected by the large standard deviation of D* in this study. Eventually, the D* and f values may be used to obtain tissue perfusion information without injection of a contrast agent, a possibility which requires further investigation.

There are several limitations in this study, including the following. (1) A relatively small population of benign cases were included in this study. (2) Lesions under 1.5 cm were not included in this study due to poor signal to noise ratio, which decreased the clinical importance of these results. (3) The number of b values was relatively small; however, we have set the maximum number of b values for the machine. (4) Since the mono- and biexponential models used different post-processing software, the ROIs cannot be copied from one model to the other; thus, the ROI cannot be guaranteed to be completely consistent. (5) Only benign and malignant lesions were compared in this study. Alternative pathological types, degrees of differentiation and biological behaviour of the lesions should be further investigated.

CONCLUSIONS

In conclusion, our preliminary study suggests that DWI- and IVIM- derived parameters may be useful in the differentiation of benign and malignant lung nodules and masses. Among them, ADC is the most robust parameter to differentiate benign and malignant lung nodules, whereas D is the most robust parameter to differentiate benign and malignant lung masses.

FUNDING

This work was supported by the Jiangsu Province High-level Health Talents "Six One Programme" Top Talent Project: LGY2017037; Yancheng medical science and technology development plan project: YK2017021; 333 High-level Talents Training Project of Jiangsu: 2016III-0603; National Key R&D Program of China: 2017YFC0114300.

REFERENCES

1. Koyama H, Ohno Y, Seki S, Nishio M, Yoshikawa T, Matsumoto S, et al. Value of diffusion-weighted MR imaging using various parameters for assessment and characterization of solitary pulmonary nodules. *Eur J Radiol* 2015; **84**: 509–15. doi: https://doi.org/10.1016/j.ejrad.2014.11.024
2. Shen G, Ma H, Liu B, Ren P, Kuang A. Diagnostic performance of DWI with multiple parameters for assessment and characterization of pulmonary lesions: a meta-analysis. *AJR Am J Roentgenol* 2018; **210**: 58–67. doi: https://doi.org/10.2214/AJR.17.18257
3. Chen L, Zhang J, Bao J, Zhang L, Hu X, Xia Y, et al. Meta-Analysis of diffusion-weighted MRI in the differential diagnosis of lung lesions. *J Magn Reson Imaging* 2013; **37**: 1351–8. doi: https://doi.org/10.1002/jmri.23939
4. Shen G, Jia Z, Deng H. Apparent diffusion coefficient values of diffusion-weighted imaging for distinguishing focal pulmonary lesions and characterizing the subtype of lung cancer: a meta-analysis. *Eur Radiol* 2016; **26**: 556–66. doi: https://doi.org/10.1007/s00330-015-3840-y
5. Henz Concatto N, Watte G, Marchiori E, Irion K, Felicetti JC, Camargo JJ, et al. Magnetic resonance imaging of pulmonary nodules: accuracy in a granulomatous disease-endemic region. *Eur Radiol* 2016; **26**: 2915–20. doi: https://doi.org/10.1007/s00330-015-4125-1
6. Le Bihan D, Breton E, Lallemand D, Aubin ML, Vignaud J, Laval-Jeantet M. Separation of diffusion and perfusion in intravoxel incoherent motion MR imaging. *Radiology* 1988; **168**: 497–505. doi: https://doi.org/10.1148/radiology.168.2.3393671
7. Deng Y, Li X, Lei Y, Liang C, Liu Z. Use of diffusion-weighted magnetic resonance imaging to distinguish between lung cancer and focal inflammatory lesions: a comparison of intravoxel incoherent motion derived parameters and apparent diffusion coefficient. *Acta Radiol* 2016; **57**: 1310–7. doi: https://doi.org/10.1177/0284185115586091
8. Wan Q, Deng Y-S, Zhou J-X, Yu Y-D, Bao Y-Y, Lei Q, et al. Intravoxel incoherent motion diffusion-weighted MR imaging in assessing and characterizing solitary pulmonary lesions. *Sci Rep* 2017; **7**: 43257. doi: https://doi.org/10.1038/srep43257
9. Weller A, Papoutsaki MV, Waterton JC, Chiti A, Stroobants S, Kuijer J, et al. Diffusion-Weighted (DW) MRI in lung cancers: ADC test-retest repeatability. *Eur Radiol* 2017; **27**: 4552–62. doi: https://doi.org/10.1007/s00330-017-4828-6
10. Jiang J, Yin J, Cui L, Gu X, Cai R, Gong S, et al. Lung cancer: short-term reproducibility of intravoxel incoherent motion parameters and apparent diffusion coefficient at 3T. *J Magn Reson Imaging* 2018; **47**: 1003–12. doi: https://doi.org/10.1002/jmri.25820
11. Griswold MA, Jakob PM, Heidemann RM, Nittka M, Jellus V, Wang J, et al. Generalized autocalibrating partially parallel acquisitions (grappa. *Magn Reson Med* 2002; **47**: 1202–10. doi: https://doi.org/10.1002/mrm.10171
12. Wang L-li, Lin J, Liu K, Chen C-zhong, Liu H, Lv P, et al. Intravoxel incoherent motion diffusion-weighted MR imaging in differentiation of lung cancer from obstructive lung consolidation: comparison and correlation with pharmacokinetic analysis from dynamic contrast-enhanced MR imaging. *Eur Radiol* 2014; **24**: 1914–22. doi: https://doi.org/10.1007/s00330-014-3176-z
13. Coolen J, Vansteenkiste J, De Keyzer F, Decaluwé H, De Wever W, Deroose C, et al. Characterisation of solitary pulmonary lesions combining visual perfusion and quantitative diffusion MR imaging. *Eur Radiol* 2014; **24**: 531–41. doi: https://doi.org/10.1007/s00330-013-3053-1
14. Fritzsche KH, Neher PF, Reicht I, van Bruggen T, Goch C, Reisert M, et al.

MITK diffusion imaging. *Methods Inf Med* 2012; **51**: 441–8. doi: https://doi.org/10.3414/ME11-02-0031
15. Sun J, Yu X, Jiaerken Y, Song R, Huang P, Wang C, et al. The relationship between microvasculature in white matter hyperintensities and cognitive function. *Brain Imaging Behav* 2017; **11**: 503–11. doi: https://doi.org/10.1007/s11682-016-9531-8
16. Koh D-M, Collins DJ, Orton MR. Intravoxel incoherent motion in body diffusion-weighted MRI: reality and challenges. *AJR Am J Roentgenol* 2011; **196**: 1351–61. doi: https://doi.org/10.2214/AJR.10.5515
17. Fujima N, Sakashita T, Homma A, Shimizu Y, Yoshida A, Harada T, et al. Advanced diffusion models in head and neck squamous cell carcinoma patients: Goodness of fit, relationships among diffusion parameters and comparison with dynamic contrast-enhanced perfusion. *Magn Reson Imaging* 2017; **36**: 16–23. doi: https://doi.org/10.1016/j.mri.2016.10.024
18. Austin JH, Müller NL, Friedman PJ, Hansell DM, Naidich DP, Remy-Jardin M, et al. Glossary of terms for CT of the lungs: recommendations of the nomenclature Committee of the Fleischner Society. *Radiology* 1996; **200**: 327–31. doi: https://doi.org/10.1148/radiology.200.2.8685321
19. Surov A, Meyer HJ, Wienke A. Correlation between apparent diffusion coefficient (ADC) and cellularity is different in several tumors: a meta-analysis. *Oncotarget* 2017; **8**: 59492–9. doi: https://doi.org/10.18632/oncotarget.17752
20. Yuan M, Zhang Y-D, Zhu C, Yu T-F, Shi H-B, Shi Z-F, et al. Comparison of intravoxel incoherent motion diffusion-weighted MR imaging with dynamic contrast-enhanced MRI for differentiating lung cancer from benign solitary pulmonary lesions. *J Magn Reson Imaging* 2016; **43**: 669–79. doi: https://doi.org/10.1002/jmri.25018
21. Das SK, Yang DJ, Wang JL, Zhang C, Yang HF. Non-Gaussian diffusion imaging for malignant and benign pulmonary nodule differentiation: a preliminary study. *Acta Radiol* 2017; **58**: 19–26. doi: https://doi.org/10.1177/0284185116639763
22. Cui L, Yin J-B, Hu C-H, Gong S-C, Xu J-F, Yang J-S. Inter- and intraobserver agreement of ADC measurements of lung cancer in free breathing, breath-hold and respiratory triggered diffusion-weighted MRI. *Clin Imaging* 2016; **40**: 892–6. doi: https://doi.org/10.1016/j.clinimag.2016.04.002
23. Çakmak V, Ufuk F, Karabulut N. Diffusion-Weighted MRI of pulmonary lesions: comparison of apparent diffusion coefficient and lesion-to-spinal cord signal intensity ratio in lesion characterization. *J Magn Reson Imaging* 2017; **45**: 845–54. doi: https://doi.org/10.1002/jmri.25426
24. Usuda K, Sagawa M, Motono N, Ueno M, Tanaka M, Machida Y, et al. Diagnostic performance of diffusion weighted imaging of malignant and benign pulmonary nodules and masses: comparison with positron emission tomography. *Asian Pac J Cancer Prev* 2014; **15**: 4629–35. doi: https://doi.org/10.7314/APJCP.2014.15.11.4629
25. Bickel H, Pinker K, Polanec S, Magometschnigg H, Wengert G, Spick C, et al. Diffusion-Weighted imaging of breast lesions: Region-of-interest placement and different ADC parameters influence apparent diffusion coefficient values. *Eur Radiol* 2017; **27**: 1883–92. doi: https://doi.org/10.1007/s00330-016-4564-3
26. Yuan M, Zhong Y, Zhang Y-D, Yu T-F, Li H, Wu J-F. Volumetric analysis of intravoxel incoherent motion imaging for assessment of solitary pulmonary lesions. *Acta Radiol* 2017; **58**: 1448–56. doi: https://doi.org/10.1177/0284185117698863
27. Wan Q, Deng Y-S, Lei Q, Bao Y-Y, Wang Y-Z, Zhou J-X, et al. Differentiating between malignant and benign solid solitary pulmonary lesions: are intravoxel incoherent motion and diffusion kurtosis imaging superior to conventional diffusion-weighted imaging? *Eur Radiol* 2019; **29**: 1607–15. doi: https://doi.org/10.1007/s00330-018-5714-6
28. Razek AAKA. Diffusion magnetic resonance imaging of chest tumors. *Cancer Imaging* 2012; **12**: 452–63. doi: https://doi.org/10.1102/1470-7330.2012.0041
29. Kakite S, Dyvorne H, Besa C, Cooper N, Facciuto M, Donnerhack C, et al. Hepatocellular carcinoma: short-term reproducibility of apparent diffusion coefficient and intravoxel incoherent motion parameters at 3.0T. *J Magn Reson Imaging* 2015; **41**: 149–56. doi: https://doi.org/10.1002/jmri.24538
30. Lemke A, Laun FB, Simon D, Stieltjes B, Schad LR. An in vivo verification of the intravoxel incoherent motion effect in diffusion-weighted imaging of the abdomen. *Magn Reson Med* 2010; **64**: 1580–5. doi: https://doi.org/10.1002/mrm.22565
31. Andreou A, Koh DM, Collins DJ, Blackledge M, Wallace T, Leach MO, et al. Measurement reproducibility of perfusion fraction and pseudodiffusion coefficient derived by intravoxel incoherent motion diffusion-weighted MR imaging in normal liver and metastases. *Eur Radiol* 2013; **23**: 428–34. doi: https://doi.org/10.1007/s00330-012-2604-1